IOP Conf. Series: Materials Science and Engineering **304** (2018) 012014 doi:10.1088/1757-899X/304/1/012014

Monte Carlo simulation and fundamental quantities

F Salvat[1] and X Llovet[2]

[1] Facultat de Física (FQA and ICC). Universitat de Barcelona. Diagonal 645, ES-08028 Barcelona, Spain
[2] Scientific and Technological Centres. Universitat de Barcelona. Lluís Solé i Sabarís, 1-3. ES-08028 Barcelona, Spain

E-mail: francesc.salvat@ub.edu

Abstract. Physics interaction models suited for Monte Carlo simulation of coupled electron-photon transport in EPMA and other spectroscopic techniques are briefly described. The considered models are required to be applicable to any material and valid for a wide energy range. Differential cross-sections, the fundamental quantities in Monte Carlo simulation, are presented for the relevant interactions of photons and electrons with energies up to about 500 keV. Approximations and simplifications underlying the interaction models and the particle tracking scheme are discussed.

1. Introduction

It is generally believed that Monte Carlo (MC) simulation provides the most accurate description of the coupled transport of electrons and photons in the energy range of interest in electron-probe microanalysis (EPMA), X-ray fluorescence (XRF), and other X-ray spectroscopic techniques. Although automatic Monte Carlo quantification tools are not widely available, simulation studies have been used to calculate EPMA spectra and characteristic X-ray yields from bulk samples, k-ratios from thin films on substrates, secondary fluorescence near planar interfaces, and the lateral resolution of EPMA measurements [1].

Indeed, MC simulation has distinct advantages over alternative numerical (finite-difference) methods. Firstly, it can describe arbitrary interaction processes, with an accuracy limited only by that of the adopted interaction models, i.e., by the adopted differential cross-sections (DCSs). Secondly, MC simulation is able to track particles through material systems with complex geometries, where deterministic methods would find great difficulties even to define the appropriate boundary conditions. Finally, the stochastic nature of MC methods permits the straightforward evaluation of statistical (type A) uncertainties of simulation results, while numerical methods allow only rough estimations of accumulated errors.

However, MC simulation methods are not free from simplifications and approximations, which limit their applicability and the reliability of the results. A fundamental simplification refers to the structure of the material where radiation propagates, which is assumed to be homogeneous and isotropic, with defined composition and density. The atoms or molecules in the medium are considered to be randomly distributed with uniform density (crystalline ordering is ignored) and molecular aggregation effects are disregarded, i.e., molecules are regarded as sets of individual atoms with *uncorrelated* positions. Only in the case of inelastic collisions of charged particles, molecular binding and aggregation effects are partially accounted for by using empirical values

of the mean excitation energies of materials, so as to ensure the correct high-energy collision stopping power. Also implicit in any MC code is the assumption that the various interaction mechanisms are effectively independent; reality is more complex, and the co-existence of multiple time-evolution paths leads to quantum interference effects (such as inelastic absorption and radiative effects in elastic collisions of charged particles), which are frequently disregarded, or treated approximately as corrections to the DCSs of the dominant interactions.

In MC simulations, the trajectories of transported (primary and secondary) particles are generated as sequences of connected free flights, each flight ending by an interaction that may change the energy and direction of the particle. This trajectory picture is justified only for high-energy radiation, whose de Broglie wavelengths are much smaller than the average separation between the atoms in the medium. When the wavelength is comparable to the interatomic distances, interference effects, resulting from the coherent superposition of waves scattered by different atoms, may become important and invalidate the trajectory picture. In addition, the tracking of particles is performed as if they were moving in an infinite, limitless medium having the local composition; this way of operation implies that interfaces are considered to be passive (thus excluding, e.g., surface plasmon excitations).

In the present article we describe physics interaction models suited for MC simulation of coupled electron-photon transport, with the focus on the fundamental quantities and on the underlying assumptions (and simplifications) that determine the reliability of the simulation results. The relevant fundamental quantities are the interaction DCSs, which describe each interaction mechanism, the corresponding total (integrated) cross-sections, and the atomic transition probabilities and energies, which determine the X-rays and Auger electrons released in the relaxation of atoms with vacancies in inner sub-shells. The interaction models described here have been implemented in the general-purpose MC code PENELOPE [2]. More detailed information on theoretical aspects can be found in the article by Salvat and Fernández–Varea [3]. More recently, a review article on electron-impact ionisation and X-ray emission has been published by Llovet *et al.* [4].

Owing to the wide energy range of interest, interactions are described using relativistic quantum mechanics. For electrons (mass $\mathrm{m_e}$, charge $-e$) with kinetic energy E and momentum $\mathbf{p} = \hbar\mathbf{k}$ ($\hbar$ is the reduced Planck constant), we will frequently use the quantities

$$\gamma \equiv \frac{E + \mathrm{m_e}c^2}{\mathrm{m_e}c^2} = \sqrt{\frac{1}{1-\beta^2}} \qquad \text{and} \qquad \beta = \frac{v}{c} = \sqrt{\frac{E(E+2\mathrm{m_e}c^2)}{(E+\mathrm{m_e}c^2)^2}} = \sqrt{\frac{\gamma^2-1}{\gamma^2}}, \tag{1}$$

which are, respectively, the total energy in units of the rest energy $\mathrm{m_e}c^2$ and the velocity in units of the speed of light c. The wave number and wavelength of the electron are

$$k = (c\hbar)^{-1}\sqrt{E(E+2\mathrm{m_e}c^2)} \qquad \text{and} \qquad \lambda = \frac{2\pi}{k} = \frac{12.398\ \text{Å}}{\sqrt{(E/\text{keV})[(E/\text{keV})+1022]}}, \tag{2}$$

respectively. The corresponding quantities for a photon of energy E are

$$k = (c\hbar)^{-1}E \qquad \text{and} \qquad \lambda = \frac{12.398\ \text{Å}}{E/\text{keV}}. \tag{3}$$

2. Interaction processes

A projectile particle (electron or photon) of energy E can interact with matter through a number of different mechanisms. In the energy-range of interest in EPMA and other X-ray spectroscopies (say from 500 eV to 500 keV), photons interact through the following processes:

◦ photelectric absorption (ph),
◦ incoherent Compton scattering (Co), and
◦ coherent Rayleigh scattering (Ra).
The relevant interaction mechanisms of electrons are:
◦ elastic collisions (el),
◦ inelastic collisions (in), and
◦ bremsstrahlung photon emission (br).

Each individual interaction may involve a certain energy transfer W to the material, a change in direction of the projectile, and, occasionally, the prompt emission of a secondary particle. For the sake of concreteness, we assume that before the interaction the projectile moves in the direction of the z axis; the direction of motion after the interaction (as well as the directions of any secondary particles released) are described by the polar and azimuthal angles, θ and ϕ, respectively (see fig. 1). Each interaction process (pr) is described in terms of the so-called differential inverse mean free path (DIMFP), $\mathrm{d}^2\mu_{\mathrm{pr}}(E)/(\mathrm{d}W\,\mathrm{d}\Omega)$, which gives the probability density of having an interaction with energy loss W and angular deflection $\Omega = (\theta, \phi)$ per unit path length of the projectile. Because of the assumed isotropy of the medium, the DIMFP is independent of the azimuthal scattering angle ϕ. The inverse mean free path, defined by

$$\mu_{\mathrm{pr}}(E) = \int \mathrm{d}W \int \mathrm{d}\Omega\, \frac{\mathrm{d}^2\mu_{\mathrm{pr}}(E)}{\mathrm{d}W\,\mathrm{d}\Omega}\,, \tag{4}$$

gives the interaction probability per unit path length of the projectile. Its reciprocal is the mean free path between interactions of that type. The energy loss and the angular deflection in an interaction are random variables with joint probability density given by

$$P_{\mathrm{pr}}(E; W, \theta, \phi) = \frac{1}{\mu_{\mathrm{pr}}(E)}\,\frac{\mathrm{d}^2\mu_{\mathrm{pr}}(E)}{\mathrm{d}W\,\mathrm{d}\Omega}. \tag{5}$$

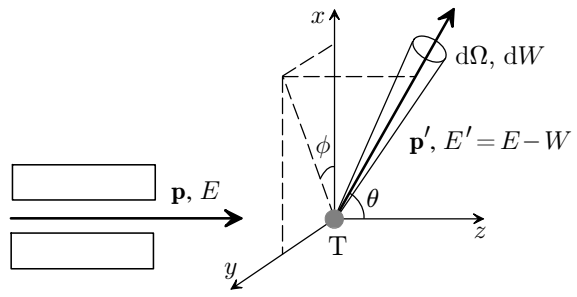

Figure 1. Schematic diagram of an experiment to measure the DCS. Incident particles move in the direction of the z axis; θ and ϕ are the polar and azimuthal scattering angles, respectively.

The details of the DIMFPs for condensed materials depend on the composition and structure (or state of aggregation) of the medium. However, when the de Broglie wavelength of the projectile [for electrons, $\lambda_{\mathrm{B}} = (150\ \mathrm{eV}/E)^{1/2}$ Å] is much less than the inter-atomic distances, the DIMFPs are nearly independent of the molecular or solid structure. Under these circumstances, the DIMFP can be estimated in terms of the atomic DCSs, $\mathrm{d}^2\sigma_{\mathrm{pr}}(Z, E)/(\mathrm{d}W\,\mathrm{d}\Omega)$, of the elements present by means of the additivity approximation. Concretely, the DIMFP for a compound (or mixture) with n_i atoms of the element of atomic number Z_i per molecule is

$$\frac{\mathrm{d}^2\mu_{\mathrm{pr}}(E)}{\mathrm{d}W\,\mathrm{d}\Omega} = \mathcal{N}\sum_i n_i \frac{\mathrm{d}^2\sigma_{\mathrm{pr}}(Z_i, E)}{\mathrm{d}W\,\mathrm{d}\Omega}, \tag{6}$$

where $\mathcal{N}$ is the number of molecules per unit volume. For a material of mass density ϱ and "molecular weight" $A_{\rm w}$ (g/mol), $\mathcal{N} = N_{\rm A}\varrho/A_{\rm w}$, where $N_{\rm A}$ is Avogadro's number. Most general-purpose MC codes utilise the additivity approximation with atomic DCSs defined by numerical databases or given by analytical formulas. The approximation is acceptable for elastic interactions. It is not accurate for inelastic collisions of charged particles, because these are dominated by excitations of conduction and valence electrons whose response depend strongly on the structure of the medium. Compton scattering of photons and photoelectric absorption also present a certain dependence on the state of aggregation. In the following we assume that the additivity approximation, with appropriate corrections, is applicable. That is, we consider interactions of electrons and photons with individual atoms of an element of atomic number Z.

A fundamental quantity, which characterises the response of the material to external electromagnetic fields and the distribution of energy losses in small-angle inelastic collisions of charged particles, is the optical dielectric function $\epsilon(\omega)$, a complex function of the angular frequency ω of the field. It is related to the familiar refraction index, $n(\omega)$, and extinction coefficient, $\kappa(\omega)$, by

$$n(\omega) + {\rm i}\kappa(\omega) = \sqrt{\epsilon(\omega)}, \tag{7}$$

where the branch of the square root is the one yielding a non-negative $n(\omega)$. The main source of measured optical dielectric functions is the *Handbook of Optical Constants of Solids* [5–7], which includes tables of $n(\omega)$ and $\kappa(\omega)$ for a number of metals, semiconductors and insulators. These tables contain measured data obtained with different methods, frequently by various groups and with various degrees of accuracy, and cover ranges of excitation energies $W = \hbar\omega$ from about 10^{-3} eV up to an upper energy that depends on the material, typically about 100 eV. For solids for which experimental information is not available, approximate optical functions can be obtained from density-functional theory calculations (see, e.g., [8]).

Because of the scarcity of experimental data, most MC codes use atomic DCSs that are either given by analytical formulas derived from simple models and approximations or defined by numerical databases generated by first-principles calculations. The latter are also affected by a number of approximations. Typically they are based on a relativistic independent-electron model of the atom, in which atomic electrons are assumed to move independently in a common central potential $V(r)$, and atomic wave functions are represented as single Slater determinants built with one-electron central-field orbitals $\psi_i(\mathbf{r})$ that are solutions of the Dirac equation with the eigenvalues E_i. Notice that the one-electron energy spectrum consists of a discrete set of levels ($E_i < 0$) corresponding to bound orbitals, and a continuum ($E > 0$) associated to free orbitals. Many calculations use the self-consistent Dirac-Hartree-Fock-Slater (DHFS) model of the atom (see, e.g., [9]). Compared with the more elaborate Dirac-Fock model [10], DHFS has the advantages of giving one-electron eigenvalues E_i in closer agreement with experimental sub-shell binding energies (see [3]) and of ensuring orthonormality of bound and free one-electron orbitals. The target atom is characterised by its ground-state configuration, i.e., by the set of electron sub-shells Si that are occupied, the number of electrons in each subshell, and the corresponding binding energies $U_i = -E_i$.

2.1. Photon interactions

• Photoelectric effect

In the photoelectric effect a photon is absorbed by the target atom and an atomic electron is excited to an empty orbital, bound or free, leaving a vacancy in the active sub-shell. Subsequently, the atom relaxes to its ground state by a sequence of radiative and non-radiative transitions.

Theoretical calculations using the independent-electron approximation (see [9] and references therein) give the partial cross-sections $\sigma_{\rm ph}({\rm S}i, E)$ for the electron sub-shells of the atom. The

atomic cross-section is the sum of contributions of the various sub-shells,

$$\sigma_{\rm ph}(E) = \sum_i \sigma_{\rm ph}({\rm S}i, E). \tag{8}$$

Most databases give cross-sections for ionisation only, that is, they exclude excitations to bound levels which are very sensitive to aggregation effects. Because photoabsorption is then forbidden for sub-shells with binding energy U_i higher than E, the total cross-section presents abrupt absorption edges. A peculiar feature of the photoeffect is that absorption occurs preferentially in the innermost sub-shell, i.e., in the sub-shell with the highest binding energy U_i that is less than E.

Extensive tables of atomic photoelectric cross-sections are given in the Evaluated Photon Data Library (EPDL) [11], which contain partial sub-shell cross-sections and total atomic cross-sections for all the elements from hydrogen ($Z = 1$) to lawrencium ($Z = 103$) and photon energies E from 10 eV to 100 GeV. For energies from the absorption edge up to 1 MeV, the tabulated cross-sections were computed with the DHFS atomic model using a computer programme of Scofield [12]. For energies higher than 1 MeV, the calculated sub-shell cross-sections were rescaled to match the total cross-sections of Hubbell *et al.* [13]. The XCOM programme [14] gives total atomic cross-sections for photon energies between 1 keV and 100 GeV, which are essentially the same as in the EPDL. Tables of total atomic cross-sections, generated from a compilation of experimental data and theoretical calculations, were published by Henke *et al.* [15] for the elements $Z = 1 - 92$ and for photon energies from 50 eV to 30 keV. Recently, Sabbatucci and Salvat [9] reformulated the theory of the atomic photoeffect to allow the easy calculation of photoelectron angular distributions. They used the DHFS model to generate a complete database, which includes total atomic cross-sections for all elements ($Z = 1$–100) and partial cross-sections for the K-shell and for the L-, M-, and N-sub-shells with binding energies higher than about 50 eV. This database is used in the MC code PENELOPE.

As noted above, atomic calculations do not account for aggregation effects. Photoelectric cross-sections for atoms in molecules and solids differ from the free-atom cross-section mostly because photoelectrons interact with neighbour atoms producing the so-called X-ray absorption fine structure (XAFS), a series of near-edge resonances together with an oscillatory component that decreases with the kinetic energy of electrons and extends up to a few-hundred eV above the edge energy [16]. For photons of small and moderate energies, and for materials with known optical dielectric functions, the photoabsortion cross-section can be obtained from the dielectric function as

$$\sigma_{\rm ph}(E) = \frac{2\omega}{\mathcal{N}c}\,\kappa(\omega), \tag{9}$$

where $\omega = E/\hbar$ is the angular frequency of photons with energy E. For energies E higher than about 100 eV, $n(\omega) \simeq 1$, $\kappa(\omega) \ll 1$, and

$$\sigma_{\rm ph}(E) \simeq \frac{\omega}{\mathcal{N}c}\,{\rm Im}[\epsilon(\omega)]. \tag{10}$$

This relation shows that calculated atomic photoelectric cross-sections can be used to define the dielectric function for frequencies higher than those attainable in measurements.

• Compton scattering

In Compton scattering the incident photon is absorbed by an atomic electron, which is promoted to an empty orbital (bound or free), and a secondary photon is emitted with energy $E' < E$ in a direction forming an angle θ with that of the incident photon. Energy conservation implies that electrons in a sub-shell Si can be excited only if $E - E' - U_i$ is larger than the energy of the lowest empty level.

The DCS for Compton scattering of unpolarised photons by free electrons at rest is given by the Klein-Nishina formula (see, e.g., [17])

$$\frac{\mathrm{d}\sigma^{(\mathrm{KN})}}{\mathrm{d}\Omega} = r_\mathrm{e}^2 \frac{1}{2} \frac{E'^2}{E^2} \left(\frac{E}{E'} + \frac{E'}{E} - \sin^2\theta \right). \tag{11}$$

Because of energy-momentum conservation, the energy E' of the scattered photon depends only on the polar scattering angle θ, and is given by

$$E' = \frac{E}{1 + (E/\mathrm{m_e}c^2)(1 - \cos\theta)} \equiv E_\mathrm{C}. \tag{12}$$

The Klein–Nishina DCS provides an acceptable description of Compton scattering for those interactions where the energy transfer is much larger than the binding energy of the active electron.

A more realistic description is obtained from the impulse approximation [18], which assumes that the electrons in the active shell Si react essentially as if they were moving with a distribution of velocities represented by the so-called Compton profile, a quantity defined as an integral of the Fourier transform of the atomic orbitals. The motion of the atomic electrons implies that the frequency of the incident photon is Doppler shifted when observed from a Lorentz frame moving with the same velocity as the target electron. The effect of binding is to prevent transitions that would lead the active electron to final bound orbitals. Note that interactions where the final state of the electron is an unoccupied bound orbital are also possible. These interactions correspond to Raman scattering (see, e.g., [19]), a process that involves relatively small energy transfers and is usually disregarded in MC codes. The impulse approximation correctly predicts that photons scattered in directions forming an angle θ with the direction of incidence have a continuous energy distribution, with a maximum near the Compton energy E_C, eq. (12). The DCS for Compton scattering by electrons in the active shell Si obtained from the impulse approximation is given by a complicated expression, that depends on the energy transfer $W = E - E'$ and the direction of the scattered photon. Adding the contributions from the various electron sub-shells and integrating over the energy of the scattered photon, the atomic DCS can be expressed as

$$\frac{\mathrm{d}\sigma_\mathrm{Co}(Z,E)}{\mathrm{d}\Omega} = \frac{\mathrm{d}\sigma^{(\mathrm{KN})}}{\mathrm{d}\Omega} S_\mathrm{inc}(Z;q), \tag{13}$$

where $S_\mathrm{inc}(Z;q)$ is the incoherent-scattering function, which depends on the momentum transfer

$$q \sim \frac{1}{c}\sqrt{E^2 + E_\mathrm{C}^2 - 2EE_\mathrm{C}\cos\theta}. \tag{14}$$

The total atomic cross-section for Compton scattering is

$$\sigma_\mathrm{Co}(Z,E) = \int \frac{\mathrm{d}\sigma_\mathrm{Co}(Z,E)}{\mathrm{d}\Omega}\,\mathrm{d}\Omega = 2\pi \int_{-1}^{1} \frac{\mathrm{d}\sigma_\mathrm{Co}(Z,E)}{\mathrm{d}\Omega}\,\mathrm{d}(\cos\theta). \tag{15}$$

The DCSs for Compton scattering adopted in PENELOPE are based on the impulse approximation, with an analytical approximation to the subshell Compton profiles. To account, at least partially, for aggregation effects the Compton profile of valence and conduction electrons may be replaced by that of an electron gas with the same density (number of electrons per unit volume) as in the material.

• Rayleigh scattering

Rayleigh scattering is the process in which the incident photon is absorbed by the target atom and a secondary photon is emitted without excitation of the target atom. Since the recoil energy of the target is very small, the secondary photon has approximately the same energy E as the projectile.

The atomic DCS for Rayleigh scattering of unpolarised photons is given by

$$\frac{\mathrm{d}\sigma_{\mathrm{Ra}}}{\mathrm{d}\Omega} = r_{\mathrm{e}}^2 \, \frac{1+\cos^2\theta}{2} \, \left| F(Z,q) + f' + \mathrm{i}f'' \right|^2 , \tag{16}$$

where

$$F(Z,q) = \int \rho(r) \, \exp(\mathrm{i}\mathbf{q}\cdot\mathbf{r}/\hbar) \, \mathrm{d}\mathbf{r} = \frac{4\pi}{q} \int_0^\infty \rho(r) \, \sin(qr/\hbar) \, r \, \mathrm{d}r. \tag{17}$$

is the atomic form factor, i.e., the Fourier transform of the atomic electron density $\rho(r)$. Tables of atomic form factors have been published by Hubbell *et al.* [20] and are included in the EPDL [11].

The quantity $f'+\mathrm{i}f''$, the so-called anomalous-scattering factor, accounts for the fast variation of the Rayleigh cross-section for photon energies around absorption edges. The tables of Henke *et al.* [15] include anomalous scattering factors for the elements Z = 1–92 and photon energies between 50 eV and 30 keV. An extensive tabulation of anomalous scattering factors, covering all the elements from hydrogen to fermium (Z = 1 to 100) and energies from 1 eV to 10 MeV has been prepared by Cullen *et al.* [21].

• Mass attenuation coefficients

The primary quantity for simulating photon histories is the (linear) attenuation coefficient, the reciprocal of the mean free path. It is given by

$$\mu = \mathcal{N}\sigma_{\mathrm{T}}, \tag{18}$$

where $\mathcal{N}$ is the number of atoms (or molecules) per unit volume and $\sigma_{\mathrm{T}} = \sigma_{\mathrm{ph}} + \sigma_{\mathrm{Co}} + \sigma_{\mathrm{Ra}}$ is the total interaction cross-section of an atom (or molecule). Assuming that the additivity approximation is applicable, the dependence of μ on the density of the material is practically removed by considering the mass attenuation coefficient,

$$\mu/\varrho = (N_{\mathrm{A}}/A_{\mathrm{w}}) \, \sigma_{\mathrm{T}}. \tag{19}$$

To give an indication of the relative importance of the different interaction processes, fig. 2 shows total and partial mass attenuation coefficients of photons in aluminium and iodine as functions of the photon energy.

2.2. Electron interactions

• Elastic collisions

By definition, elastic collisions are interactions of the projectile electron that leave the initial state of the target atom unaltered. In an elastic collision the trajectory of the incident electron is deflected, with a very small energy transfer (of the order of a few meV) to the target atom, which recoils after the interaction.

Most MC codes describe elastic collisions by means of DCSs calculated by the relativistic (Dirac) partial-wave expansion method, with a central potential $V(r)$ that represents the electrostatic interaction energy between the projectile and the charge distribution of the target atom, which is assumed to remain "frozen" during the interaction (static-field approximation), plus a generally small correction to account for electron exchange effects. The programme

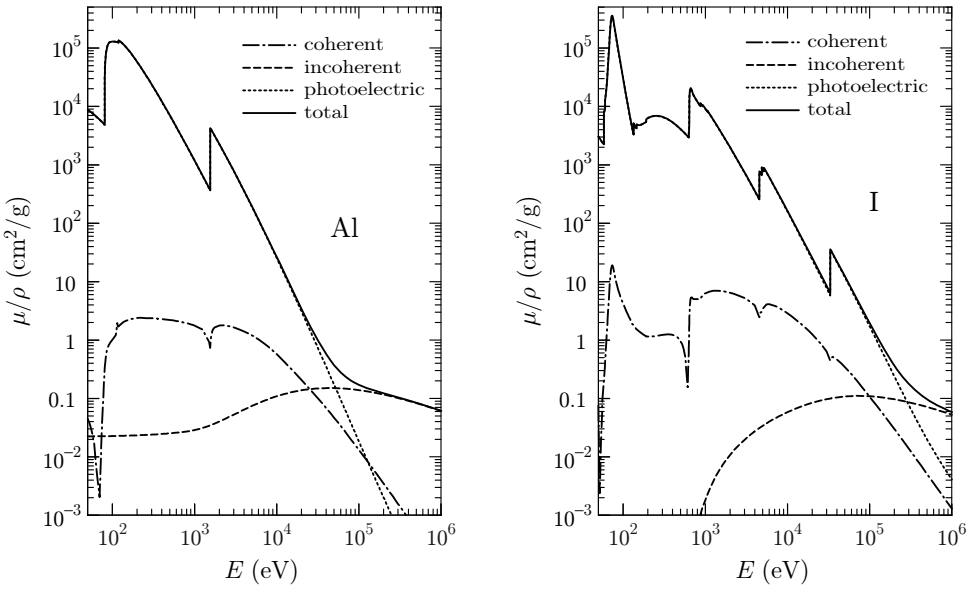

Figure 2. Partial and total mass attenuation coefficients of aluminium metal and iodine as functions of the photon energy. Notice the different low-E behaviour of $\mu_{\rm Co}/\rho$ for insulators (iodine) and conductors (aluminium).

ELSEPA of Salvat *et al.* [22], performs these calculations for electrons and positrons with kinetic energies up to $\sim$ 100 MeV.

The ICRU Report 77 [23] gives a review of theoretical calculation methods and experimental measurements of elastic scattering of electrons and positrons. This report includes an extensive database of DCSs for elastic scattering of projectiles with kinetic energies from 50 eV to 100 MeV by atoms of the elements $Z = 1$ to 103, which was generated by running ELSEPA. It is worth mentioning that DCSs calculated from the partial-wave expansion method are systematically larger than the measured DCSs (see, e.g., [24]) because of inelastic absorption effects (electrons that undergo inelastic interactions are effectively removed from the elastic channel) and also because of radiative corrections [25]. Inelastic absorption reduces the DCS by up to 10 percent in extreme cases. In principle, this correction is accounted for in MC simulations that include a detailed description of inelastic collisions. The static-field approximation fails for low-energy projectiles and small scattering angles, because the electric field of the projectile polarises the charges of the target atom, and the induced dipole acts back on the projectile. This polarisation correction can be described by including an extra term in the interaction potential, but it is usually disregarded in MC simulations on the grounds that small scattering angles do not have much influence on the whole transport process.

In old MC codes it was usual to describe elastic collisions by using the DCS obtained from the Born approximation, which is given by

$$\frac{{\rm d}\sigma_{\rm el}}{{\rm d}\Omega} = \frac{1-\beta^2\sin^2(\theta/2)}{1-\beta^2}\left(\frac{2{\rm m_e}z_0e^2}{q^2}\right)^2\left[Z-F(Z,q)\right]^2 \qquad (20)$$

where $F(Z,q)$ is the atomic form factor, eq. (17), and

$$q = 2p\sin(\theta/2) \tag{21}$$

is the momentum transfer.

• Inelastic collisions

The theoretical description of inelastic collisions of electrons, and other charged particles, is intrinsically difficult, because of the strong correlations between the energy loss W and the scattering angle θ. The basic theory of the process is based on the first-order plane wave Born approximation (PWBA) in which the effective interaction between the projectile and the target atom is treated as a perturbation to first order, with the initial and final states of the projectile represented as plane waves. The physics of the process is shown more explicitly when the DCS is expressed in terms of the energy loss W and the recoil energy Q defined by (see [26])

$$Q(Q + 2\mathrm{m_e}c^2) = (cq)^2 = c^2\left(p^2 + p'^2 - 2pp'\,\cos\theta\right) \tag{22}$$

where $\mathbf{q} = \mathbf{p} - \mathbf{p}'$ is the momentum transfer ($\mathbf{p}'$ is the momentum of the projectile after the collision). Note that Q equals the relativistic kinetic energy of an electron with momentum equal to the momentum transfer. Evidently, when the energy transfer is much larger than the binding energies U_i of the atomic electrons, these react essentially as if they where free and at rest and, consequently, the most probable excitations are those with $W \simeq Q$. A formal derivation with an independent-electron approximation (see [27]) yields a formula for the DCS which, after neglecting terms that are small for projectiles with energies $\lesssim 500$ keV, reads

$$\begin{aligned}\frac{\mathrm{d}^2\sigma_{\mathrm{in}}}{\mathrm{d}W\,\mathrm{d}Q} &= \frac{2\pi e^4}{\mathrm{m_e}v^2}\left[\frac{2\mathrm{m_e}c^2}{WQ(Q+2\mathrm{m_e}c^2)}\right.\\ &\left.+\left(\beta^2 - \frac{W^2}{Q(Q+2\mathrm{m_e}c^2)}\right)\frac{W\,2\mathrm{m_e}c^2}{[Q(Q+2\mathrm{m_e}c^2)-W^2]^2}\right]\frac{\mathrm{d}f(Q,W)}{\mathrm{d}W},\end{aligned} \tag{23}$$

where v is the velocity of the projectile. The last factor, the so-called generalised oscillator strength (GOS), is defined by an infinite sum of matrix elements of the operator $\exp(\mathrm{i}\,\mathbf{q}\cdot\mathbf{r}/\hbar)$ between orbitals describing the initial and final states of the target electron; the atomic GOS is obtained as the sum of partial GOSs for the various subshells of the target atom. The GOS is independent of the charge and energy of the projectile and embodies a complete description of the dynamics of the interaction (within the PWBA). Bote and Salvat [27] have calculated a complete database of sub-shell GOSs for the elements (Z = 1–99) using DHFS one-electron orbitals.

It is worth mentioning that the PWBA is formally equivalent to a semi-classical formulation in terms of the dielectric function $\epsilon(k,\omega)$, a function of the wave number $k = q/\hbar$ and the angular frequency $\omega = W/\hbar$, which describes the response of the material to external electromagnetic fields. In the limit $k \to 0$, $\epsilon(k,\omega)$ reduces to the optical dielectric function, i.e., $\epsilon(\omega) = \epsilon(k=0,\omega)$. The so-called optical-data models combine empirical optical data with various approximate forms of the dielectric function of the degenerate electron gas to build a model of $\epsilon(k,\omega)$ for finite wave numbers k. The classical theory determines the stopping force on the projectile from the Maxwell equations. The semi-classical interpretation of the quantities $\hbar k$ and $\hbar\omega$ as, respectively, the momentum transfer and the energy loss, allows extracting an expression of the DIMFP. This semi-classical DIMFP is essentially equivalent to the result from the PWBA if one makes the identification

$$\frac{\mathrm{d}f(Q,W)}{\mathrm{d}W} \equiv W\left(1 + \frac{Q}{\mathrm{m_e}c^2}\right)\frac{2Z}{\pi\Omega_{\mathrm{p}}^2}\,\mathrm{Im}\left(\frac{-1}{\epsilon(k,\omega)}\right), \tag{24}$$

where

$$\Omega_{\mathrm{p}} = \sqrt{4\pi\mathcal{N}Z\frac{\hbar^2 e^2}{\mathrm{m_e}}} \tag{25}$$

is the plasma resonance energy of an electron gas with the average electron density of the medium. The clear advantage of optical-data models is that, apart from experimental uncertainties of the adopted optical dielectric function, they describe the actual response of the medium, including the effects of aggregation.

The energy-loss DCS is

$$\frac{\mathrm{d}\sigma_{\mathrm{in}}}{\mathrm{d}W} \equiv \int_{Q_-}^{Q_+} \frac{\mathrm{d}^2\sigma_{\mathrm{in}}}{\mathrm{d}W\,\mathrm{d}Q}\,\mathrm{d}Q, \tag{26}$$

where Q_- and Q_+ are the minimum and maximum kinematically allowed recoil energies, which are given by eq. (22) with $\cos\theta = \pm 1$. The total cross-section is the integral of the energy-loss DCS over allowed energy transfers. The collision (or electronic) stopping power S_{col} is defined as the average energy loss per unit path length due to inelastic collisions, and is given by

$$S_{\mathrm{col}} = -\frac{\mathrm{d}E}{\mathrm{d}s} = \mathcal{N}\int_0^{W_{\max}} W\,\frac{\mathrm{d}\sigma_{\mathrm{in}}}{\mathrm{d}W}\,\mathrm{d}W, \tag{27}$$

where $\mathcal{N}$ is the number of atoms or molecules per unit volume and $W_{\max}$ is the maximum allowed energy transfer. When the energy E of the projectile is much larger than the binding energies of the atomic electrons, the stopping power is given by the celebrated Bethe formula,

$$S_{\mathrm{col}} = \mathcal{N}\,\frac{2\pi e^4}{\mathrm{m_e}v^2}\,Z\left\{\ln\left(\frac{E^2}{I^2}\,\frac{\gamma+1}{2}\right) + \gamma^{-2}\left[1 - (2\gamma-1)\ln 2 + \frac{1}{8}\,(\gamma-1)^2\right]\right\}, \tag{28}$$

where I is the mean excitation energy, defined by

$$Z\ln I = \int_0^{\infty} \ln W\,\frac{\mathrm{d}f(0,W)}{\mathrm{d}W}\,\mathrm{d}W. \tag{29}$$

This quantity has been determined empirically for a large number of materials (see [28] and references therein) from measurements of the stopping power of heavy charged particles and/or from experimental optical dielectric functions. Most MC codes make explicit use of these empirical I values. For materials not included in the ICRU tables [28], I is usually estimated from the additivity approximation. Figure 3 shows stopping powers of electrons in aluminium, silver and gold metals generated by the PENELOPE code. Notice that the Bethe formula (28) is accurate only for energies higher than about 10 keV.

The ionisation of inner atomic shells by electron impact is the main source of X-rays in EPMA. The PWBA yields accurate ionisation cross-sections for electrons with energy higher than about 30 times the binding energy of the active shell. At lower energies, the distortion of the projectile wave functions by the electrostatic field of the target atom, and electron exchange effects, become important. A more elaborate theoretical description of total ionisation cross-sections is obtained from the relativistic distorted-wave Born approximation (DWBA), which consistently accounts for these effects (see e.g., [27] and references therein). DWBA calculations yield total cross-sections in fairly good agreement with measurements for ionisation of K-, L- and M-shells (see [4]). These calculations involve the expansion of free-state wave functions as partial wave series and the subsequent evaluation of multiple radial integrals. Since the convergence of partial-wave series worsens with increasing kinetic energies, DWBA calculations are feasible only for projectiles with relatively small energies, up to about 30 U_i.

The NIST Standard Reference Database 164 [29] contains an extensive numerical tabulation of ionisation cross-sections for K-, L- and M-shells of all the elements from hydrogen ($Z = 1$) to einsteinium ($Z = 99$), for electrons and positrons with kinetic energies from threshold up to 1 GeV, which was calculated by combining the DWBA and the PWBA as described by Bote and Salvat [27]. Also, analytical formulas for the easy calculation of these cross-sections were published by Bote *et al.* [30,31]. These formulas are coded in a simple Fortran programme that yields cross-sections that agree with those in the numerical database to within about 1 %. The PENELOPE database also includes ionisation cross-sections for N-shells of heavy elements, which were calculated using the same methodology as for the K-, L- and M-shells. Total cross-sections for impact ionisation of the K-, L-, and M-shells of gold are shown in fig. 3.

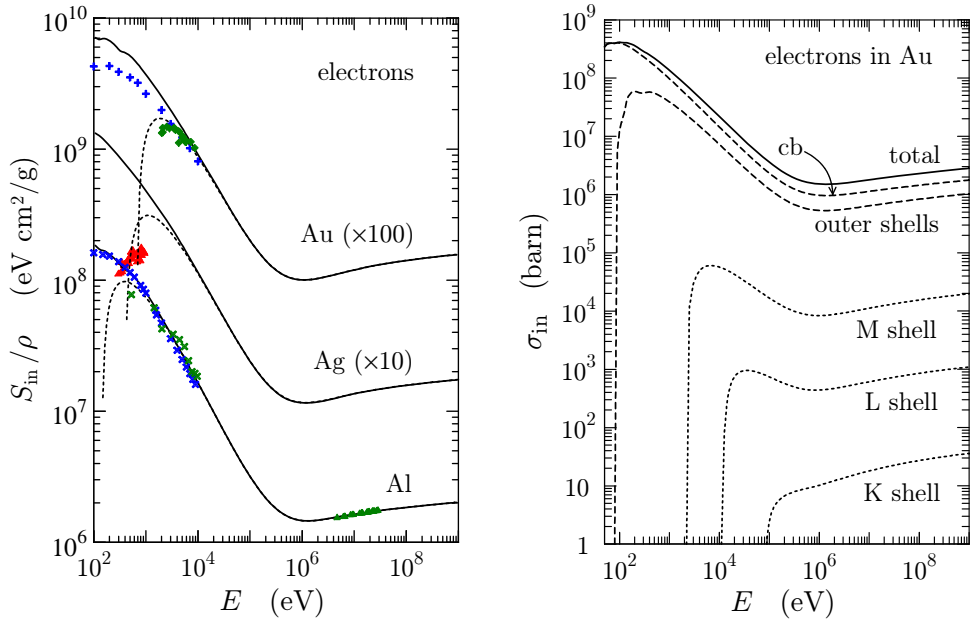

Figure 3. Left: Collision stopping powers of aluminium, silver and gold as functions of the kinetic energy E of the projectile electron. Symbols represent experimental data from different authors. The dotted curves are the stopping powers obtained from the Bethe formula, eq. (28). Right: Sub-shell cross-sections and total cross-section for inelastic collisions of electrons in gold, generated by the PENELOPE code. The dotted curves represent total ionisation cross-sections for the K-, L- and M-shells from the NIST database [29]. Solid curves represent total stopping powers and inelastic cross-sections used in PENELOPE.

• Bremsstrahlung emission

Bremsstrahlung emission is caused by the interaction of the projectile electron with the electrostatic field of the atom or in collisions with atomic electrons. The theory of the process is reviewed in the book of Haug and Nakel [32].

In MC codes the energy of emitted quanta is sampled from an energy-loss DCS, differential in only the energy W of the emitted photon, expressed in the form

$$\frac{{\rm d}\sigma_{\rm br}}{{\rm d}W} = \frac{Z^2}{\beta^2}\,\frac{1}{W}\,\chi(Z,E,\kappa). \tag{30}$$

where $\chi(Z,E,\kappa)$, the so-called scaled DCS, is a function of the atomic number Z, the energy of the projectile E, and the reduced energy of the photon, $\kappa \equiv W/E$. For a given element, this

function is finite and varies smoothly with E and κ. Seltzer and Berger [33, 34] have prepared extensive tables of bremsstrahlung energy spectra, obtained by combining different theoretical models, for electrons with kinetic energies E from 1 keV to 10 GeV incident on neutral atoms of the elements $Z = 1 - 100$.

To complete the simulation of bremsstrahlung emission events, one has to determine the direction of the emitted photon. The angular distribution of emitted photons in electron-nucleus bremsstrahlung (the so-called shape function) has been calculated by Kissel *et al.* [35], using a partial-wave expansion method, for 144 combinations of atomic number Z, electron energy E, and reduced photon energy κ. Acosta *et al.* [36] found that these shape functions can be closely approximated as Lorentz-boosted dipole distributions, from which the emission angle can be sampled analytically.

In the case of compounds, with n_i atoms of the element Z_i per molecule, the molecular DCS is obtained by means of the additivity approximation,

$$\frac{\mathrm{d}\sigma_{\mathrm{br}}}{\mathrm{d}W} = \sum_i n_i \frac{Z_i^2}{\beta^2} \frac{1}{W} \chi(Z_i, E, \kappa). \tag{31}$$

It is worth noticing that the total cross-section for bremsstrahlung emission is infinite, due to the divergence of the DCS at $W = 0$. In MC simulation we consider only the emission of photons with energies higher than a certain cutoff W_{c}, and the associated total cross-section

$$\sigma_{\mathrm{br}}(W > W_{\mathrm{c}}) = \int_{W_{\mathrm{c}}}^{E} \frac{\mathrm{d}\sigma_{\mathrm{br}}}{\mathrm{d}W} \mathrm{d}W \tag{32}$$

is finite. The radiative stopping power

$$S_{\mathrm{rad}} = \mathcal{N} \int_0^E W \frac{\mathrm{d}\sigma_{\mathrm{br}}}{\mathrm{d}W} \mathrm{d}W = \mathcal{N} \int_0^E W \left(\sum_i n_i \frac{Z_i^2}{\beta^2} \chi(Z_i, E, \kappa) \right) \mathrm{d}W, \tag{33}$$

is finite. Tables of radiative stopping powers, obtained from Seltzer and Berger's scaled DCSs, are given in Ref. [28].

2.3. Atomic relaxation

Interactions of photons and electrons that cause the emission of secondary electrons (photoelectric absorption, Compton scattering of photons, and inelastic collisions of electrons) leave the target atom ionised and in an excited state. The excited ion then relaxes to its ground state through a sequence of radiative and non-radiative transitions, in which photons (fluorescence X-rays) and Auger electrons are emitted, respectively. Atomic relaxation can be simulated by using information from the LLNL Evaluated Atomic Data Library (EADL) of Perkins *et al.* [37], which provides a comprehensive tabulation of transition probabilities and energies for both radiative and non-radiative transitions for all elements. The transition probabilities in this library were calculated theoretically by assuming that the relaxing ion has a single vacancy (an assumption that ceases to hold, e.g., after a non-radiative transition) and transition energies were approximated by means of the DHFS energy eigenvalues for neutral atoms. PENELOPE simulates atomic relaxation using transition probabilities and Auger-electron energies from the EADL. However, the energies of X-rays emitted in radiative transitions are taken from the compilations of experimental values by Deslattes *et al.* [38], for K- and L-lines, and by Bearden [39], for M-lines. In the case of radiative transitions not included in these compilations (e.g., N-lines), the EADL X-ray energies are adopted.

A common practice in studies of X-ray emission is to consider cross sections for emission of characteristic X-rays, $\sigma^{\mathrm{x}}_{\mathrm{S0,S1}}$, defined so that the product $\mathcal{N}\sigma^{\mathrm{x}}_{\mathrm{S0,S1}}$ equals the probability of

emission of an S0-S1 X-ray per unit path length of the projectile. These cross-sections can be measured by counting the emitted S0-S1 X-rays when projectile electrons of energy E impinge on a very thin foil of the material. $\sigma^{\mathrm{x}}_{\mathrm{S0,S1}}$ can be expressed as a weighted sum of electron-impact ionisation cross-sections for the sub-shell S0, and for inner sub-shells, with weights determined by the appropriate partial widths and fluorescence and Coster-Kronig yields. Detailed formulas for the emission cross-sections of K-, L- and M-lines are given, e.g., by Llovet *et al.* [4].

3. Approximations in MC simulation

Within a MC code random particle histories are simulated from the initial energy of primary particles down to a certain cutoff, the absorption energy E_{abs}, at which the particles are considered to be effectively absorbed in the material. Secondary particles that are emitted as a direct result of the interaction, and also in the relaxation of atoms following inner-shell ionisation (by photoelectric absorption and Compton scattering of photons and by electron impact) may be stored in memory and tracked subsequently in the same way as the primary particles.

The simulation of photons can be performed by the usual detailed procedure, where all interaction events in a photon history are simulated in chronological succession. That is, a photon of energy E starts from a certain position, $\mathbf{r}_0$, determined in accordance to the characteristics of the radiation source, moving in a direction defined by the unit vector $\hat{\mathbf{d}}_0$. The distance s to the next interaction is determined by random sampling from the exponential distribution

$$p(s) = \mu(E)\, \exp[-s\mu(E)], \tag{34}$$

where $\mu(E)$ is the IMFP of the photon. The particle is then moved the distance s along the ray, i.e., to a position $\mathbf{r} = \mathbf{r}_0 + s\hat{\mathbf{d}}_0$, where the next interaction takes place. The type of the next interaction is sampled according to the total cross-sections of the possible interaction mechanisms, and the interaction is simulated from the corresponding DCS. In Rayleigh and Compton scattering, the photon is absorbed by electrons in the medium and a second photon is emitted with energy E' (equal or less than E). When $E' > E_{\mathrm{abs}}$, the surviving photon is followed by repeating these steps. Photoabsorption terminates the photon history. Each history is a sequence of a relatively small number of free flights and interactions, which can be simulated rapidly.

This simulation scheme can be readily adapted to real situations, with material structures that may consist of several regions of different compositions separated by mathematical surfaces (interfaces). Photons are simulated in the current material as described above, and when they reach an interface, the tracking is discontinued and resumed with the cross-sections of the new material. That is, to track photons in complex geometries, we only need to determine the distances at which a ray intersects the interfaces.

In principle, electrons can also be tracked using detailed simulation. However, because the average energy loss in each collision is of the order of a few tens of eV, the number of interactions undergone by an electron may be quite large and detailed simulation is inefficient. The code PENELOPE utilises a more efficient tracking strategy that combines detailed simulation of hard events (i.e., interactions with scattering angle or energy loss larger than pre-defined cutoffs) and approximate multiple-scattering methods for describing the accumulated effect of the (usually many) soft interactions that occur between two consecutive hard events. Other codes may have recourse to more drastic approximations, which speed up the simulation at the expense of simplifying the interaction physics. For instance, EPMA codes may use the continuous-slowing-down approximation (CSDA), which consists in assuming that electrons lose energy continuously, at the rate prescribed by the stopping power. Although this approximation yields reasonable results for homogeneous samples, it may introduce considerable distortions for specimens with inclusions at depths slightly larger than the effective range.

Individual interaction events should be simulated by random sampling from the associated DCSs. However, the DCSs for Compton scattering of photons and inelastic collisions of electrons depend explicitly on the energy transfer W and the scattering angle θ (or the recoil energy Q). These variables are strongly correlated and, in addition, the DCSs vary rapidly with the energy of the projectile. Such DCSs are not practicable for MC simulation, not only because of the large memory required to store the numerical DCS (a three-dimensional table) but also because random sampling from multivariate distributions is far more complicated, and slower, than from univariate distributions. A frequent practice is to disregard (or alter artificially) correlations between variables, normally by sampling the most relevant quantity from its marginal probability distribution and using approximate probability distributions for the other variables. Approximations of this kind are employed in virtually all MC codes; they are harmless in the majority of applications, but they can cause visible distortions of the simulation results in cases where particles undergo a small number of interactions (e.g., in transmission through thin foils).

In the MC code PENELOPE inelastic collisions are described by using a simple GOS model consisting of discrete resonances, which reproduces the adopted total cross-sections for ionisation of inner sub-shells and the empirical value of the mean excitation energy I. This model yields very accurate stopping powers at high energies, and the correct number of inner-shell ionisations per unit path length. It also provides a realistic description of energy-loss fluctuation in individual collisions. The description of Compton scattering in PENELOPE is based on approximate analytical forms of the sub-shell Compton profiles, which allow exact random sampling of W and θ.

4. Concluding remarks

The interaction models considered in this review provide a fairly realistic description of coupled electron-photon transport, in spite of the fact that they involve quite drastic approximations. MC simulations based on those and similar models have proved to be practically useful in EPMA and other applications involving X-rays. Still, users of general-purpose MC codes should be well aware of the limited accuracy of the method, which results from uncertainties in the adopted fundamental quantities, from the neglect of possible aggregation effects, and from simplifications in the description of the sample geometry. These limitations give rise to type B uncertainties in the results of MC simulations, which add to the (statistical) type A uncertainties typically quantified by MC codes.

Acknowledgements

Financial support from the Spanish Ministerio de Economía y Competitividad and ERDF (project ref. FPA2016-77689-C2-2-R) and from the Generalitat de Catalunya (grant 2014 SGR 846) is gratefully acknowledged.

References

[1] Llovet X and Salvat F 2017 *Microsc. Microanal.* **23** 634–646
[2] Salvat F 2015 PENELOPE-*2014: a code system for Monte Carlo simulation of electron and photon transport.* (Issy-les-Moulineaux, France: OECD/NEA Data Bank) available from `http://www.nea.fr/lists/penelope.html`
[3] Salvat F and Fernández-Varea J M 2009 *Metrologia* **46** S112–S138
[4] Llovet X, Powell C J, Jablonski A and Salvat F 2014 *J. Phys. Chem. Ref. Data* **43** 013102
[5] Palik E D (Ed.) 1985 *Handbook of optical constants of solids.* (San Diego, CA: Academic Press)
[6] Palik E D (Ed.) 1991 *Handbook of optical constants of solids II.* (San Diego, CA: Academic Press)
[7] Palik E D (Ed.) 1998 *Handbook of optical constants of solids III.* (San Diego, CA: Academic Press)
[8] Werner W S M, Glantschnig K and Ambrosch-Draxl C 2009 *J. Phys. Chem. Ref. Data* **38** 1013–1092
[9] Sabbatucci L and Salvat F 2016 *Radiat. Phys. Chem.* **121** 122–140

[10] Grant I P 1970 *Advances in Physics* **19** 747–811
[11] Cullen D E, Hubbell J H and Kissel L 1997 *EPDL97 the Evaluated Photon Data Library, '97 version. Report UCRL-50400* (Livermore, California: Lawrence Livermore National Laboratory)
[12] Scofield J H 1973 *Theoretical photoionization cross sections from 1 to 1500 keV. Report UCRL-51326* (Livermore, California: Lawrence Livermore Laboratory)
[13] Hubbell J H, Gimm H A and Øverbø I 1980 *J. Phys. Chem. Ref. Data* **9** 1023–1147
[14] Hubbell J H and Seltzer S M 1996 *Tables of X-ray mass attenuation coefficients and mass energy-absorption coefficients from 1 keV to 20 MeV for elements $Z = 1$ to 92 and 48 additional substances of dosimetric interest. NISTIR 5632 database.* (Gaithersburg, MD: National Institute of Standards and Technology) `https://www.nist.gov/pml/x-ray-mass-attenuation-coefficients`
[15] Henke B L, Gullikson E M and Davis J C 1993 *At. Data Nucl. Data Tables* **54** 181–342
[16] Rehr J J and Albers R C 2000 *Rev. Mod. Phys.* **72** 621–654
[17] Sakurai J J 1967 *Advanced quantum mechanics.* (New York: Addison and Wesley)
[18] Ribberfors R 1975 *Phys. Rev. B* **12** 2067–2074
[19] Baym G 1974 *Lectures in quantum mechanics.* (Boulder, Colorado: Westview Press)
[20] Hubbell J H, Veigele W J, Briggs E A, Brown R T, Cromer D T and Howerton R J 1975 *J. Phys. Chem. Ref. Data* **4** 471–538
[21] Cullen D E 1989 *Program SCATMAN: a code designed to calculate photon coherent scattering anomalous scattering factors and cross sections. Report UCRL-ID-103422.* (Livermore, CA: Lawrence Livermore National Laboratory)
[22] Salvat F, Jablonski A and Powell C J 2005 *Comput. Phys. Commun.* **165** 157–190
[23] ICRU Report 77 2007 *Elastic scattering of electrons and positrons.* (Bethesda, MD: ICRU)
[24] Salvat F 2003 *Phys. Rev. A* **68** 012708
[25] Motz J W, Olsen H A and Koch H W 1964 *Rev. Mod. Phys.* **36** 881–928
[26] Fano U 1963 *Ann. Rev. Nucl. Sci.* **13** 1–66
[27] Bote D and Salvat F 2008 *Phys. Rev. A* **77** 042701
[28] ICRU Report 37 1984 *Stopping powers for electrons and positrons.* (Bethesda, MD: ICRU)
[29] Llovet X, Salvat F, Pujol F S, Jablonski A and Powell C J 2014 *NIST database of cross sections for inner-shell ionization by electron or positron impact.* (Gaithersburg, MD: National Institute of Standards and Technology) available from `http://dx.doi.org/10.6028/NIST.NSRDS.164`
[30] Bote D, Salvat F, Jablonski A and Powell C J 2009 *At. Data and Nucl. Data Tables* **96** 871–909
[31] Bote D, Salvat F, Jablonski A and Powell C J 2011 *At. Data and Nucl. Data Tables* **97** 186
[32] Haug E and Nakel W 2004 *The elementary process of bremsstrahlung.* (Singapore: World Scientific)
[33] Seltzer S M and Berger M J 1985 *Nucl. Instrum. Meth. B* **12** 95–134
[34] Seltzer S M and Berger M J 1986 *At. Data Nucl. Data Tables* **35** 345–418
[35] Kissel L, Quarles C A and Pratt R H 1983 *At. Data Nucl. Data Tables* **28** 381–460
[36] Acosta E, Llovet X and Salvat F 2002 *Appl. Phys. Lett.* **80** 3228–3230
[37] Perkins S T, Cullen D E, Chen M H, Hubbell J H, Rathkopf J and Scofield J 1991 *Tables and graphs of atomic subshell and relaxation data derived from the LLNL Evaluated Atomic Data Library (EADL), $Z = 1$–100. Report UCRL-ID-50400.* (Livermore, CA: Lawrence Livermore National Laboratory)
[38] Deslattes R D, Kessler E G, Indelicato P, de Billy L, Lindroth E and Anton J 2003 *Rev. Mod. Phys.* **75** 36–99
[39] Bearden J A 1967 *Rev. Mod. Phys.* **39** 78–124